COMPARISON OF CONVENTIONAL ELASTIC AND IMAGING LIDAR SYSTEMS FOR ATMOSPHERIC AEROSOL MONITORING: A REVIEW

Sani Muhammad[1,2]*, C. J. Wong[2], Mutawalli Bello[2,3], M. A. Mohammed[1,2]
[1]Department of Physics, Federal University of Lafia, PMB 146, Nasarawa State, Nigeria
[2]School of Physics, Universiti Sains Malaysia (USM), 11800, Pulau Pinang, Malaysia
[3]Department of Physics, Federal College of Education, Yola, Adamawa State, Nigeria
*Corresponding author: elsani20@yahoo.com

Abstract: Light detection and ranging (LiDAR) system is an active remote sensing technique which operates within the optical spectral wavelength range. The ability of LiDAR to provide range-resolved information with high temporal and spatial resolution makes it suitable to be widely used in atmospheric sensing devices to measure temperature, humidity, wind speed, aerosols and/clouds, and others. This paper contains the comparison between two types of elastic LiDAR (conventional LiDAR and imaging LiDAR); their techniques, methodologies and state of the art instrumentation utilized to acquire atmospheric aerosol information in a transition to make it simple and cost effective for ease of accessibility in scientific and research community. However, it takes different degrees of instrumental sophistication to retrieve structural (aerosol layer profiling), optical (backscatter and extinction coefficients) and microphysical (size, shape and type) properties. Ground-based coordinated LiDAR networks and space borne orbiting LiDARs together will provide a better understanding of the role of aerosols and/clouds in the global radiative balance and contribute to air-quality forecasts and meteorological analyses. The up-to-dateprogress as well as the future prospect of LiDAR has been outlined in this paper.

Keywords: Atmospheric aerosol, elastic LiDAR, conventional LiDAR, imaging LiDAR, air-quality

Introduction

As an active remote sensing technique, light detection and ranging (LiDAR) system operates within optical spectral wavelength range. The LiDAR ability to provide range-resolved information with high temporal and spatial resolution makes it widely used in various atmospheric sensing such as temperature (Arshinov *et al.,* 1983; Chen *et al.,* 2004), humidity (Vaughan *et al.*, 1988; Soriano *et al.,* 1995), wind speed (Sroga *et al.,* 1980; Liu *et al.*, 2016), aerosols and clouds (Collis and Russell, 1976; Wandinger *et al.*, 2011; Liu *et al.*, 2013), among others. Over the past five decades conventional elastic (the same wavelength for both emission and detection) nanosecond-pulsed LiDAR technique based on time-of-flight approach, has proven to be an effective tool for profiling aerosol vertical structure especially in the planetary boundary layer (PBL). Aerosol optical properties (backscatter and extinction coefficients) are commonly retrieved using this LiDAR system. Apart from the conventional LiDAR system, atmospheric aerosol properties are also monitored by the recently developed imaging LiDAR technique. It uses photon angle of incidence to retrieve range-resolved information rather than the photon time of flight. The conventional LiDAR system and the imaging LiDAR system can either be of monostatic configuration or bistatic configuration, but generally monostatic one prevails in both. The two different aerosol LiDAR systems (conventional and imaging LiDAR systems) with the atmospheric aerosol properties retrieved were summarised in Tables 1 and 2.

Progress in LiDAR system depends on technological breakthroughs on mainly the laser transmitter and the receiver sub-systems, which are the core components of LiDAR instrument. In addition, as can be seen in Table 1, simple LiDAR systems which are capable of determining the aerosol structural and optical properties are traced back to 60s and 70s of the twentieth century whereas based on Table 2, the imaging LiDAR emerged recently. Conventional as well as imaging LiDAR systems developments for microphysical properties retrieval are limited to the recent two decades.

Table 1: Aerosol properties retrieved from conventional aerosol LiDAR measurements

Properties	Parameters	References
Structural	PBL height	Collis *et al.* (1964), Allen and Evans (1972) Stull (1988)
	Lofted layer base, top and thickness	Pal *et al.* (1992), Xu *et al.* (2019)
	Cloud base, top and thickness	
Optical	Backscatter coefficient	Fernald *et al.* (1972), Fernald (1984), Potter (1987), Sicard *et al.* (2002)
	Extinction coefficient	
Microphysical	Shape	Gimmestad (2008), Xie *et al.* (2015)
	Size	Chaikovsky *et al.* (2016), Lopatin *et al.* (2013), Dubovik *et al.* (2014)
		Kaufman *et al.* (2005), Shimizu *et al.* (2004), Tesche *et al.* (2009), Ansmann *et al.* (2012)

Table 2: Aerosol properties retrieved from imaging aerosol LiDAR measurements

Properties	Parameters	References
Structural	PBL height	Mei *et al.* (2019a), Mei *et al.* (2019b)
	Cloud base, top and thickness	Mei and Brydegaard (2015a)
Optical	Backscatter coefficient	Kong *et al.* (2018), Mei *et al.* (2018),
	Extinction coefficient	Sun *et al.* (2018), Mei *et al.* (2017)
Microphysical	Shape Size	Mei and Guan (2017), Zhao *et al.* (2018), Mei *et a.* (2018)

FUW Trends in Science & Technology Journal, www.ftstjournal.com
e-ISSN: 24085162; p-ISSN: 20485170; December, 2021: Vol. 6 No. 3 pp. 713 – 721

713

LiDAR systems were deployed both on the ground and in the space to provide better local and global aerosol vertical distribution properties. Space LiDARs include LITE (LiDAR In-Space Technology, space shuttle-based LiDAR); CALIOP (Cloud-Aerosol LiDAR with Orthogonal Polarisation) onboard the CALIPSO (Cloud-Aerosol LiDAR and Infrared Pathfinder Satellite Observations) satellite; CATS (Cloud–Aerosol Transport System) onboard ISS (International Space Station) and ALADIN (Atmospheric Laser Doppler LiDAR Instrument) onboard ADM-Aeolus (Atmospheric Dynamics Mission-Aeolus) (Ansmann *et al.*, 2013). EarthCARE (Earth Cloud and Aerosol Explorer) from ESA (European Space Agency) and JAXA (Japan Aerospace Exploration Agency) is planned to be launched in June, 2022.

Continuous progress in laser and detector technologies has been recorded for the last five decades. However still LiDAR system improvement can solve some important problems of atmospheric sciences, such as inaccurate profiling of atmospheric aerosols because of large uncertainties in the retrieval of their properties. It is stressed in Intergovernmental Panel on Climate Change (IPCC) reports from 2001 onward (IPCC, 2001), that aerosol properties impact on the Earth radiation budget and on the climate is poorly studied. The large spatio-temporal variations and the concentration of atmospheric aerosol properties must be considered to assess its effects on climate and air-quality. Furthermore, the cost, maintenance and instrumental complexity of LiDAR system especially conventional hindered its wider spread in the scientific research community (Barnes *et al.,* 2007; Liu *et al.*, 2019). The conventional LiDAR system, however, faces some challenges which includes afterpulse effects, high cost, incomplete receiver's field-of -view overlap and high dynamic range requirements (Harms, 1979; Campbell *et al.*, 2002). Comparatively, imaging LiDAR system has an advantage of utilizing area imaging sensors thus require no overlap factor calibration and needs low dynamic range.

The aim of this review is to provide the up-to-date state of the art in elastic LiDAR system (conventional LiDAR and imaging LiDAR) utilized for atmospheric aerosols remote sensing.

LiDAR Techniques
Conventional elastic LiDAR technique
Conventional elastic LiDAR simply means a LiDAR system emitting a wavelength and detecting radiation elastically backscattered by the atmospheric constituents at that wavelength (Takeuchi, 2005). Thus, the energy of the incident photons is conserved. Equation (1) gives the single-scattering equation for return elastic-backscatter LiDAR signal at laser wavelength λ_o (m).

$$P_{\lambda_o}(R) = \frac{K_{\lambda_o}}{R^2} O_{\lambda_o}(R)\beta_{\lambda_o}(R)T_{\lambda_o}^2(R) \qquad 1$$

$P_{\lambda_o}(R)$ is the received power (W) backscattered from range R (m), and K_{λ_o} is the system constant $\left(K_{\lambda_o} = E(\lambda_o)A_r\xi(\lambda_o)c/2\right)$ where $E(\lambda_o)$ is the pulse energy (J) at wavelength λ_o, A_r is the effective telescope receiving area (m^2), $\xi(\lambda_o)$ is the optics net transmission of the system and c is the light velocity (ms^{-1}). The term $O_{\lambda_o}(R)$ is the overlap function accounting for fractional laser beam cross-section contained by the receiver telescope field of view as a function of range R. It is determined by many different optical and geometrical parameters of the system as well as laser beam intensity distribution (Stelmaszczyk *et al*., 2005; Hey *et al.*, 2011). $\beta_{\lambda_o}(R)$ (m^{-1}sr^{-1}) is the total atmospheric backscatter coefficient, ($\beta_{\lambda_o} = \beta_{\lambda_o}^{aer} + \beta_{\lambda_o}^{mol}$) with aerosols (aer) and molecules (mol) contribution. $T_{\lambda_o}^2(R)$ is the round-trip atmospheric transmittance due to both aerosols and molecules define as (Kovalev and Eichinger, 2005):

$$T_{\lambda_o}(R) = \frac{I_{\lambda_o}(R)}{I_{\lambda_o}(0)} = \exp\left(-\int_0^R \alpha_{\lambda_o}(x)dx\right) \qquad 2$$

Where $I_{\lambda_o}(R)$ is the intensity at range R and α_{λ_o} is the total atmospheric optical extinction coefficient (m^{-1}). Light extinction occurs due to scattering and absorption by molecules and aerosols. Thus, the total extinction coefficient can be written as:

$$\alpha_{\lambda_o} = \alpha_{\lambda_o}^{aer} + \alpha_{\lambda_o}^{mol} \qquad 3$$

The independent determination of backscatter and extinction coefficients is the solution to the basic LiDAR equation. But in an elastic LiDAR system with one measured quantity, $P_{\lambda_o}(R)$ and two unknown variables (α_{λ_o} and β_{λ_o}) it is an underspecified problem (Bösenberg and Hoff, 2007).

The elastic LiDAR equation solution dates back to 1950s when radar received signal was inverted for the rate of rainfall (Hitschfeld and Bordan, 1954) and Fernald *et al.* (1972) reconsidered LiDAR equation inversion. Based on one-component atmosphere assumption, an unstable forward and stable far-end solution of LiDAR equation were presented by Davis (1969) and Klett (1981) respectively. In the LiDAR inversion algorithm introduced by Fernald (Fernald, 1984) and later reformulated by Klett (1985), the atmospheric aerosols and molecules contributions to the extinction were separated explicitly. Due to the under-determination problem of LiDAR equation, both one- component and two-component (Klett-Fernald, KF) algorithm require a calibration (boundary) value of the extinction or backscatter coefficient at the far-end of the range profile and extinction-to-backscatter ratio (so-called LiDAR ratio) as inputs. The KF algorithm is preferred because it permits the use of the aerosol-only LiDAR ratio, a parameter characterising the microphysical aerosol properties (Böckmann *et al.*, 2008). The KF backward inversion algorithm for the retrieval of aerosol backscatter coefficient at λ_o is written as (Rocadenbosch *et al.*, 2012):

$$\beta^{aer}(R) = \frac{[R^2 P(R)]\exp\left\{2\int_R^{R_m}[S^{aer}(u)-S^{mol}]\beta^{mol}(u)du\right\}}{\frac{[R_m^2 P(R_m)]}{\beta^{aer}(R_m)+\beta^{mol}(R_m)}+2\int_R^{R_m}S^{aer}(u)[u^2 P(u)]\exp\left\{2\int_u^{R_m}[S^{aer}(v)-S^{mol}]\beta^{mol}(v)dv\right\}du} - \beta^{mol}(R) \qquad 4$$
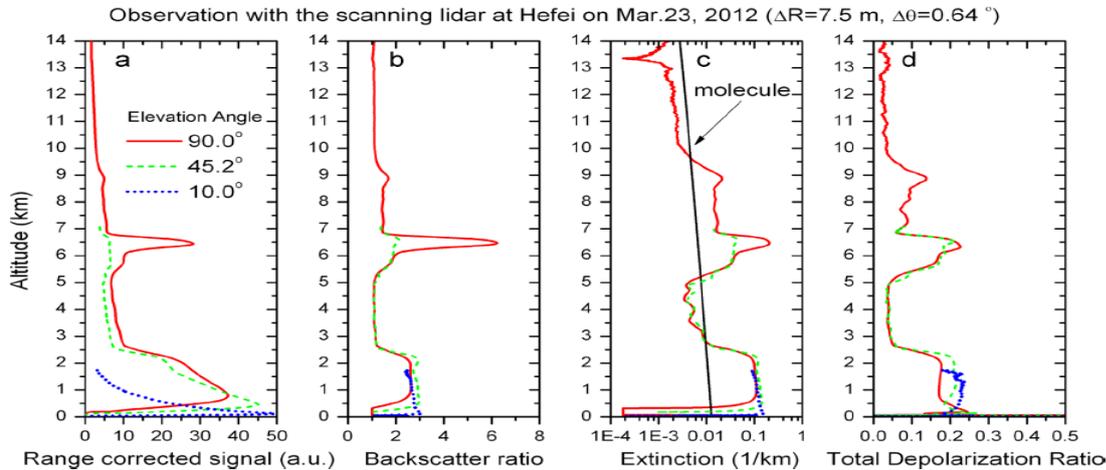
Where $P(R)$ is the return LiDAR power, $S^{aer}(R)$ and $S^{mol}(R) = \frac{8\pi}{3}$ are the aerosol and the molecular LiDAR ratios, respectively. $R_m(\ R \leq R_m)$ is the calibration range at far-end chosen such that $\beta(R_m) = \beta^{aer}(R_m) + \beta^{mol}(R_m) \approx \beta^{mol}(R_m)$. In practice, the atmospheric molecular backscatter coefficient is determined from temperature/pressure profile obtained by radiosonde or standard atmosphere model (Bodhaine *et al.*, 1999; Behrendt *et al.*, 2011). A constant (range- independent) aerosol LiDAR ratio is usually assumed based on aerosol information of the study area but is debatable for aerosol layers that varies significantly with height (Wandinger *et al.*, 2002; Mattis *et al.*, 2004). The noise and error assessment in elastic LiDAR retrieval are presented in (Comerón *et al.*, 2004; Rocadenbosch *et al.*, 2012).

A trustworthy extinction profiles are hard to achieve from elastic LiDAR backscatter coefficient retrieval. This is because the extinction profile calculation must be done by multiplying the backscatter profile retrieved with the range-independent LiDAR ratio that was used before as input in the backscatter retrieval (Bösenberg and Hoff, 2007). Numerous alternative methods have been presented which includes constraining extinction profiles with optical thickness measured using Sun photometer along the sounding path (Pedrós *et al.*, 2010), nephelometer measurement of near-end boundary value (Hoff *et al.*, 1996; Kovalev, 2003), among others.

Figure 1(a)-(d) shows the retrieved vertical profiles of the range corrected signal, backscatter ratio, extinction coefficient

FUW Trends in Science & Technology Journal, www.ftstjournal.com
e-ISSN: 24085162; p-ISSN: 20485170; December, 2021: Vol. 6 No. 3 pp. 713 – 721

714

and total depolarization ratio of aerosol and cloud observed with the scanning polarisation Mie LiDAR (SPML) system on 23 March 2012 at Hefei, China using constant LiDAR ratio of 50 sr at 532 nm wavelength (Xie *et al.*, 2015). The height of planetary boundary layer (PBL) is approximately 2.5 km and cloud occur at about 6.5 km with the LiDAR observation range of up to 14 km. The time plot of the range-corrected

LiDAR signal at 1064 nm near Manaus, Brazil is depicted in Fig. 2. Cirrus clouds were detected in the upper tropical troposphere between the 8- and 16-km heights. A lofted aerosol layer at around 2.5 and 1.5 km deep residual layer can be seen in the lower troposphere.

Fig. 1: Vertical profiles of the (a) range corrected signal, (b) backscatter ratio, (c) extinction and (d) total depolarization ratio of aerosol and cloud (Xie *et al.*, 2015)

Ceilometers are simply LiDARs. The commercial ceilometers used low-priced pulsed laser diode as transmitter with emission wavelength normally in the range 900 – 1100 nm (near infrared). Though it has high pulsed repetition frequency (few kilohertz) but with low pulse energy thereby allowing eye-safe operation. The receiver typically consists of an optical assembly (100 – 200 mm diameter) to collect the backscattered light, an avalanche photodiode (as photodetector), and a digitizer board.

The primary use of ceilometers is to determine the height of cloud base, but simple size, low operational and maintenance cost, and commercial availability geared their rapid development with establishment of large number of national weather services of its networks. They are providing data at near-real continuous time (Wiegner *et al.*, 2014; Madonna *et al.*, 2015). This deployment fostered scientific community to explore its aerosol properties retrieval capability which is currently technologically hindered. Achieving that will complement the existing advance aerosol LiDAR networks station which are spatially less dense and lacked continuous observation.

Despite the poor signal-to-noise ratio of ceilometers, an observation range of 7.5 km with 5 min and 15 m temporal and spatial resolutions respectively is typically achievable. But correct quantitative aerosol optical properties retrieval required backscatter calibration for molecular return at a reference height (aerosol-free region) which is challenging in ceilometers (Wiegner *et al.*, 2014). Thus, only aerosol vertical structural property can be derived from ceilometer measurement.

Imaging LiDAR technique

The imaging LiDAR technique has been proposed and demonstrated in both bistatic (Meki *et al.*, 1996; Barnes *et al.*, 2003) and monostatic (Mei and Brydegaard, 2015b) configuration for atmospheric aerosol profiling. The bistatic imaging LiDAR utilized wide angle lens with small aperture as the receiver and good for near range monitoring (Barnes *et al.,* 2007). The drawback of this technique is low light collection efficiency which limit it operation only to night-time. Besides that, aerosol phase function needs to be

considered as the angle of the side scatter light may differ significantly with the change in the measurement altitude (Tao *et al.*, 2014) and narrowband interference filters performed poorly in suppressing background noise due to large field of view.

In the recent years, a monostatic imaging LiDAR technique for atmospheric profiling based on Scheimflug principle is developed and is called Scheimflug LiDAR (SLiDAR) (Mei and Brydegaard, 2015b; Kong *et al.*, 2018). In contrast, SLiDAR can achieved much larger collecting efficiency of backscattering light with large aperture telescope, phase function variation is negligible and small field of view enable narrowband interference filter usage. The range domain analysis of the SLiDAR is presented (Agishev, 2020) as well as the signal measured is validated successfully by comparison studies performed with conventional elastic LiDAR (Mei *et al.*, 2019b). However, the signal-to-noise ratio (SNR) of the SLiDAR detected signal is not optimized due to the low quantum efficiency of the tilted image sensor resulting in the large angle of the incident light (Catrysse and Wandell, 2002; Dittrich *et al.*, 2019). Moreover, another monostatic imaging LiDAR is proposed (Kong *et al.*, 2020) employing parallel placed image sensor and achieved appreciable signal-to-noise ratio as compared with SLiDAR. This LiDAR technique is referred to as shallow depth-of-field imaging LiDAR (SDOFI-LiDAR) and unlike SLiDAR, the backscattering image of this SDOFI-LiDAR is defocused in the near/far range which lead to overestimation of the LiDAR signal at this range. The range-resolved backscattering signal is acquired based on the angle of backscattering light captured by the image sensor rather than the time-of-arrival. For SLiDAR, relationship between pixel position (p_I) and measurement distance (z) is deduced from geometrical optics as (Mei and Brydegaard, 2015b, 2015a):

$$z = \frac{L(p_I(\sin\Theta - \cos\Theta\tan\Phi) + L_{IL})}{p_I(\cos\Theta + \sin\Theta\tan\Phi) + L_{IL}\tan\Phi} \qquad 5$$

Where Φ is the swing angle of lens and L_{IL} is the distance between image and lens plane given by Eq. (6) and (7) respectively. L is the distance between the lens and image planes.

FUW Trends in Science & Technology Journal, www.ftstjournal.com
e-ISSN: 24085162; p-ISSN: 20485170; December, 2021: Vol. 6 No. 3 pp. 713 – 721

715

$$\Phi = \arctan \frac{L}{z_{\text{ref}}} - \arctan \frac{p_{\text{I,ref}} \cos \Theta (z_{\text{ref}} - f)}{z_{\text{ref}} f} \qquad 6$$

$$L_{\text{IL}} = \frac{z_{\text{ref}} f}{z_{\text{ref}} - f} - p_{\text{I,ref}} \sin \Theta \qquad 7$$

Here $\frac{\arctan L}{z}$ is the backscattering angle of light (γ). The values of Φ and L_{IL} can be calibrated by measuring the pixel position ($p_{\text{I,ref}}$) of the backscattering signal from a remote fixed target with known distance (z_{ref}). From Eq. (5) the range resolution (dz) of SLiDAR is deduced as:

$$Dz = -\frac{z^2 L_{\text{IL}} \cos \Theta (1 + \tan^2 \Phi)}{L \left(L_{\text{IL}} + p_{\text{I}} (\sin \Theta - \cos \Theta \tan \Phi) \right)^2} \, dp_{\text{I}} \qquad 8$$

Where dp_{I} is the pixel interval which is a constant. The range resolution (dz) of SDOFI-LiDAR is the same as that of SLiDAR Eq. (8) (at $\Theta = 0$).

The LiDAR equation for monostatic imaging LiDAR is similar to that of conventional monostatic LiDAR system, Eq. (1), except that the $\frac{1}{R^2}$ term is eliminated due to the trigonometric relationship of the system and often the overlap function is considered to be 1 because two-dimensional image sensor can fully capture the transmitted laser beam (Mei and Brydegaard, 2015b):

$$P_{\lambda_o}(R) = K_{\lambda_o} \beta_{\lambda_o}(R) \exp \left(-2 \int_0^R \alpha_{\lambda_o}(x) dx \right) \qquad 10$$

Thus, inversion algorithms of conventional elastic LiDAR can also be used in imaging LiDAR to retrieve extinction coefficient or backscattering coefficient as discuss earlier. The noise sources were modelled and assessed (Mei *et al.*, 2018) for imaging LiDAR technique. Fig. 3 depicts the aerosol extinction coefficients profiles retrieved by the Fernald method in different measurement times (August 2017) in Dalian, China using imaging LiDAR (SLiDAR) (Mei *et al.,* 2018). As can be seen, the maximum retrieval distance varies based on the different atmospheric conditions (hazy, moderately polluted or clean) from about 2 to 7 km.
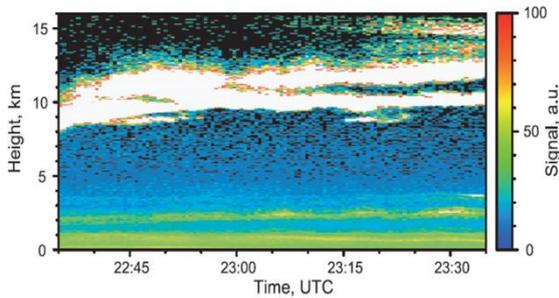

Fig. 2: Temporal plot of the range-corrected signal at 1064-nm wavelength between 2235 and 2335 UTC on 15 Aug 2008 at near Manaus, Brazil (Althausen *et al.*, 2009)
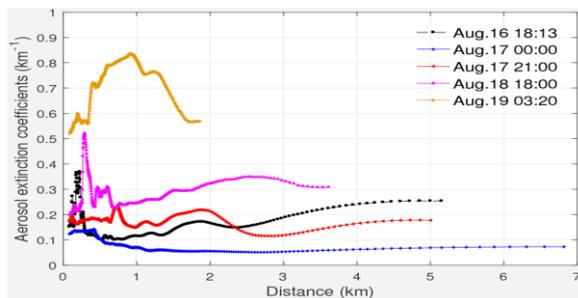

Fig. 3: Retrieved aerosol extinction coefficients by the Fernald method in different measurement times (August 2017) at Dalian, China (Mei *et al.*, 2018)
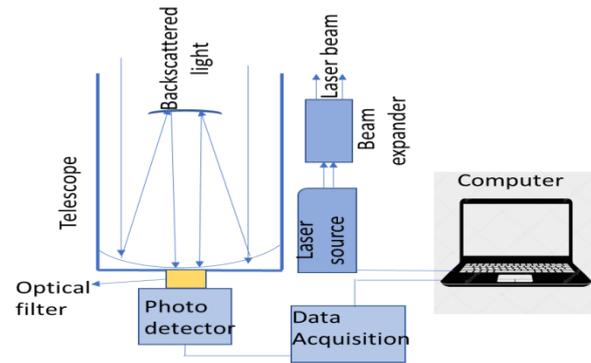

Fig. 4: The schematic of conventional LiDAR system
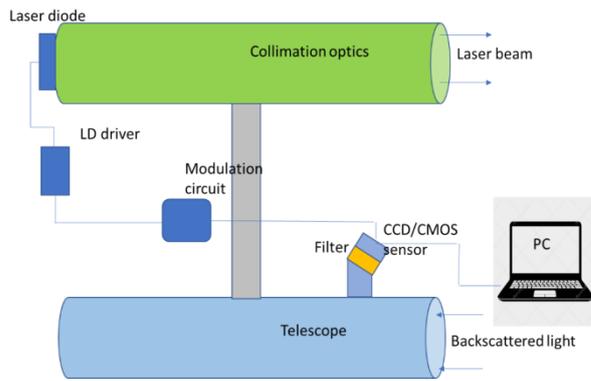

Fig. 5: The schematic of imaging LiDAR system

Instrumentation

Basically, conventional elastic LiDAR systems are made up of transmitter and receiver sub-systems co-located, with fast photodetectors and acquisition electronics as shown in Fig. 3. The transmitter is usually a powerful pulsed laser (e.g. Nd:YAG laser) for aerosol remote sensing and a telescope at the receiver serves as the collector of photons backscattered. In order to minimise background noise, the collected optical signal is filtered, converted to an electrical signal by means of a fast photodetector (e.g., photomultiplier tubes/avalanche photodiodes, PMT/APD), amplified, digitised, and stored for further processing. The construction of a conventional elastic pulsed LiDAR system is still highly expensive and complex, despite the rapid development of pulsed laser sources and photon-detection electronics; hence limit it is usage to the atmospheric research community (Barnes *et al.*, 2003; Mei and Brydegaard, 2016). In the other hand, a monostatic imaging LiDAR system has the same functional scheme as the conventional elastic LiDAR (Fig. 4) but employing a high-power continuous-wave (CW) laser diode as light source with integrated Complementary Metal Oxide Semiconductor (CMOS)/Charge-Coupled Device (CCD) sensor as the detector. This LiDAR system (Fig. 5) is relatively simple and cost-effective.

LiDAR system performance is determined primarily by wavelength of operation, laser pulse energy or power, receiver collecting area, optical throughput, out-of-band rejection ratio, as well as detector efficiency, linearity and dynamic range.

Transmitter

Conventional elastic LiDAR

The laser source is one of the core components of a LiDAR system and serves as the LiDAR transmitter as shown in Fig. 1. Progress in LiDAR instrumentation strongly depends on laser technology. However, early lasers used for remote atmospheric probing includes ruby, copper-vapor, nitrogen

and CO_2 (Killinger and Menyuk, 1987). Since 80s, high-power excimer and Nd:YAG lasers are widely utilized not only as LiDAR emitters but also to pump secondary laser sources. In LiDAR system, wavelength choice depends on application but usually the atmospheric transparent spectral region is considered as well as eye-safety and optical interaction of atmospheric constituents. Atmospheric aerosols and molecules scattering are more strong in the ultraviolet (UV) and visible wavelengths as compared with the infrared wavelength, however eye-safety is achieved most in the later (Cao *et al.*, 2009). Several conventional LiDAR have been developed for aerosol profiling (Table 3). However, these LiDARs mainly used high power pulsed Nd:YAG laser transmitter at fundamental wavelength of 1064 nm, with doubling (532 nm) and tripling (355 nm) capability using non-linear crystals (Comerón *et al.*, 2017). Even though the laser beams are well collimated, some LiDAR systems employed beam expander to further reduced the divergence of the beams and consequently allowing narrow receiver field of view (FOV) usage suppressing background light and multiple scattering detection (Wandinger, 2005). In addition, this will mitigate eye damage somewhat (Pal *et al.*, 2005). The laser beam is transmitted into the atmosphere after beam expansion. However, the high-power pulsed lasers used in conventional elastic LiDARs are of high cost and sophisticated though covering large distances.

Imaging LiDAR

The inherent conventional high power pulsed lasers were maintained as transmitters in bistatic imaging LiDAR for atmospheric aerosols profiling (Meki *et al.*, 1996; Barnes *et al.*, 2007; Sharma *et al.*, 2011). Meanwhile the advancement in laser technology make high power CW laser diodes widely available and relatively cheap in the recent years at different wavelengths ranging from 405 to 1550 nm (Brydegaard *et al.*, 2017). These lasers are utilized in monostatic imaging LiDAR systems as light sources for atmospheric aerosols and trace gases monitoring recently, e.g., at 407, 450, 520, 532 and 808 nm (Mei and Brydegaard, 2015c, 2016; Kong *et al.*, 2018, 2020; Mei *et al.*, 2018; Sun *et al.*, 2018; Mei *et al.*, 2019b) as evident in Table 3. The large divergence of laser diode beam can be reduced using cylindrical lens pair to improve geometrical transmission efficiency (Kong *et al.*, 2018).

Table 3: Different transmitter parameters specification for conventional and Imaging LiDAR systems; PRF = pulse repetition frequency

Wavelength (nm)	Pulse energy (mJ)	PRF (kHz)	Pulse Duration (ns)	Beam divergence (mrad)	Output power (W)	Ref.
532	500	0.03	5-7	0.5		Moorgawa *et al.* (2007)
1574	150-200	0.01	9	<5		Cao *et al.* (2009)
1064, 532	0.435	10				Marchant (2009)
532	120	0.015		1.5		Althausen *et al.* (2009)
1064	400	0.03	7	0.1		Liu *et al.* (2011)
355	300	0.03	5	1		Behrendt *et al.* (2011)
355	16	0.02	7			Lolli *et al.* (2011)
1064, 532	150	0.01	6			Strawbridge (2013)
532	100	0.02				Xie *et al.* (2015)
532	200	0.2		0.5		Lihui *et al.* (2015)
532	160	0.01		0.6		Meki *et al.* (1996)
532	330	0.03	8	<1		Barnes *etal.* (2007)
CW laser diode 808				$38^0 \perp \times 10^0 \parallel$	3.2	Mei and Brydegaard (2015b)
CW laser diode 450				$45^0 \perp \times 14^0 \parallel$	3.5	Kong *et al.* (2018)
CW laser diode 407				$45^0 \perp \times 13^0 \parallel$	1	Mei *et al.* (2018)
CW laser diode 520					1	Mei *et al.* (2019)
CW laser diode 808					4	Liu *et al.* (2019)

Table 4: Receiver parameters specification for conventional and Imaging LiDAR systems

Telescope diameter (mm)	Telescope focal length (mm)	Detector	Filter	Resolution (pixels)	Ref.
445	2000	PMT			Moorgawa *et al.* (2007)
361.9		APD, PIN			Cao *et al.* (2009)
280		PMT, APD			Marchant (2009)
200		PMT	523nm: 1nm FWHM		Althausen *et al.* (2009)
450		PMT, APD	1064nm: 0.3nm FWHM		Liu *et al.* (2011)
400	4000	PMT	355nm: 8nm FWHM		Behrendt *et al.* (2011)
					Lolli *et al.* (2011)
354	3910	PMT, APD			Strawbridge (2013)
220		PMT	532nm: 0.3nm FWHM		Xie *et al.* (2015)
230		PMT			Lihui *et al.* (2015)
		CCD	532nm: 3nm FWHM	510x492	Meki *et al.* (1996)
		CCD	532nm: 10nm FWHM	512x512	Barnes *et al.* (2007)
200	800	CMOS	808nm: 3nm FWHM	2088x1088	Mei and Brydegaard (2015b)
200	800	CMOS	450nm: 10nm FWHM	2048x1024	Kong *et al.* (2018)
200	800	CMOS	407nm: 1.7nm FWHM	2048x1024	Mei *et al.* (2018)
200	800	CMOS	520nm: 10nm FWHM	2048x1024	Mei *et al.* (2019a)
150	750	CMOS		2048x1024	Liu *et al.* (2019)

FUW Trends in Science & Technology Journal, www.ftstjournal.com
e-ISSN: 24085162; p-ISSN: 20485170; December, 2021: Vol. 6 No. 3 pp. 713 – 721

717

Receiver conventional elastic LiDAR

The receiver subsystem of an elastic LiDAR system may include receiver optics (usually telescope), the optical analyser, the fast photodetectors, and data acquisition electronics. Table 4 summarised the specifications of some parameters for the components (both conventional elastic LiDAR and imaging LiDAR). The laser beam backscattered by the atmospheric constituents (aerosols and molecules) are collected and focused to a smaller spot with the telescope. The reflective (mirror) telescope is preferred over refractive (lens) one mostly of primary diameter of 0.1 to few meters depending on whether higher atmosphere or lower atmosphere is to be probed (Wandinger, 2005).

In conventional elastic LiDAR, optical analysis of the backscattered signal is usually performed prior to detection. This is simply done using interference filter to suppress light outside transmission band such as background light from reaching the detector to avoid saturation and higher noise levels. A depolarisation sensitive elastic system has additional spectral analysis carry out by polarization analysers. The filtered backscattered light is detected (converted to electrical signal) commonly using PMT (particularly at ultraviolet and visible wavelengths for its superior signal-to-noise ratio) or APD (at infrared wavelength for its sensitivity) (Agishev *et al.*, 2006). However, the signal detection can be based on photon counting mode when backscattered signal is weak for far distance or analog detection mode for strong backscattered signal from short distance. The average current from the PMT in analog detection mode is converted to digital form using fast analog-to-digital converter (ADC) for further processing and storage.

Imaging LiDAR

The receiver and/or detector components in an imaging LiDAR system are mainly telescope and an imaging sensor. This imaging sensor used as detectors can be CCD or CMOS camera sensor. The telescope focused the entire illuminating volume onto an area imaging sensor, thus overcoming the overlap and dynamic range problems as well as necessity for scanning of conventional elastic LiDAR system (Barnes *et al.*, 2007). An interference filter is usually employed to supress the sunlight background radiation. Meanwhile the expensive detectors and data acquisition electronics of conventional elastic LiDAR is avoided by utilizing the CMOS/CCD camera sensor for the purpose, thus making imaging LiDAR relatively inexpensive (Kong *et al.*, 2018).

Conclusions

The atmospheric LiDARs are proved to be strong tools for range-resolved atmospheric remote sensing. Advances in laser and LiDAR technology aided the improvement particularly in aerosol LiDARs. Conventional elastic aerosol LiDARs have attained a greater level of maturity but imaging aerosol LiDARs are still at development stage propelled by the strong interest in providing wider aerosol properties coverage at affordable cost. Thus, ground-based coordinated LiDAR networks and spaceborne orbiting LiDARs together will provides a good understanding of the role of aerosols and/clouds in the global radiative balance and contribute to air-quality forecasts and meteorological analyses.

References

Agishev R, Gross B, Moshary F, Gilerson A& Ahmed S 2006. Simple approach to predict APD/PMT lidar detector performance under sky background using dimensionless parametrization. *Opt. and Lasers in Eng.*, 44(8): 779–796. doi: 10.1016/j.optlaseng.2005.07.010.

Agishev RR 2020. CW range-resolved S-lidars: capabilities and limitations in range domain. *Opt. and Lasers in Engr.*, 134: 106260–68. doi: 10.1016/j.optlaseng.2020.106260.

Allen RJ and Evans WE 1972. Laser radar (LIDAR) for mapping aerosol structure. *Rev. Sci. Instruments*, 43(10): 1422–1432. doi: 10.1063/1.1685458.

Althausen D, Engelmann R, Baars H, Heese B, Ansmann A, Müller D & Komppula M 2009. Portable raman lidar pollyxt for automated profiling of aerosol backscatter, extinction, and depolarization. *J. Atmos. and Oceanic Tech.*, 26(11): 2366–2378. doi: 10.1175/2009JTECHA1304.1.

Ansmann A, Seifert P, Tesche M & Wandinger U 2012. Profiling of fine and coarse particle mass: Case studies of Saharan dust and Eyjafjallajökull/Grimsvötn volcanic plumes. *Atmos. Chem. and Phy.*, 12(20): 9399–9415. doi: 10.5194/acp-12-9399-2012.

Ansmann A, Müller D, Wandinger U & Mamouri RE 2013. Lidar profiling of aerosol optical and microphysical properties from space: overview, review, and outlook. *1st Inter. Conf. on Rem Sensing and Geoinfo. Env.*, 8795: 8795021–9. doi: 10.1117/12.2028112.

Arshinov YF, Bobrovnikov SM, Zuev VE & Mitev VM 1983. Atmospheric temperature measurements using a pure rotational Raman lidar. *Applied Opt.*, 22(19): 2984. doi: 10.1364/ao.22.002984.

Barnes JE, Bronner S, Beck R & Parikh NC 2003. Boundary layer scattering measurements with a charge-coupled device camera lidar. *Applied Opt.*, 42(15): 2647. doi: 10.1364/ao.42.002647.

Barnes JE, Sharma NCP & Kaplan TB 2007. Atmospheric aerosol profiling with a bistatic imaging lidar system. *Applied Opt.*, 46(15): 2922–2929. doi: 10.1364/AO.46.002922.

Behrendt A, Pal S, Wulfmeyer V, Valdebenito B, Álvaro M & Lammel G2011. A novel approach for the characterization of transport and optical properties of aerosol particles near sources - Part I: Measurement of particle backscatter coefficient maps with a scanning UV lidar.*A tmos. Env.*, 45(16): 2795–2802. doi: 10.1016/j.atmosenv.2011.02.061.

Böckmann C *et al.* 2008. From EARLINET-ASOS raman-lidar signals to microphysical aerosol properties via advanced regularizing software. *Int. Geosci. and Remote Sensing Symposium (IGARSS)*, 2(1). doi: 10.1109/IGARSS.2008.4779018.

Bodhaine BA,Wood NB, Dutton EG & Slusser JR 1999. On rayleigh optical depth calculations. *J. Atmos and Oceanic Tech.*, 16: 1854–1861.

Bösenberg J & Hoff RM 2007. Plan for the implementation of the GAW Aerosol Lidar Observation Network (GALION). *World Meteorological Organization*, 178: 53.

Brydegaard M, Malmqvist E, Jansson S, Zhao G, Larsson J & Török S 2017. The Scheimpflug lidar method. *Proc. of SPIE.*, 10406:104060|1-17. doi: 10.1117/12.2272939.

Campbell JR, Hlavka DL,Welton EJ, Flynn CJ, Turner DD, Spinhirne JD, Stanley S & HwangIH2002. Full-time, eye-safe cloud and aerosol lidar observation at atmospheric radiation measurement program sites: Instruments and data processing. *J. Atmos and Oceanic Tech.*, 19(4): 431–442. doi: 10.1175/1520-0426(2002)019<0431:FTESCA>2.0.CO;2.

Cao N, Zhou X, Li S & Chen Z 2009. A new eye-safe lidar design for studying atmospheric aerosol distributions. *Rev. Sci. Instrum.*, 80(3): 0351091-9. doi: 10.1063/1.3103647.

Catrysse PB & Wandell BA 2002. Optical efficiency of image sensor pixels. *J. of OSA A.*, 19(8): 1610–20. doi: 10.1364/josaa.19.001610.

FUW Trends in Science & Technology Journal, www.ftstjournal.com
e-ISSN: 24085162; p-ISSN: 20485170; December, 2021: Vol. 6 No. 3 pp. 713 – 721

718

Chaikovsky A, Dubovik O, Holben B, Bril A, Goloub P, Tanré D, Pappalardo G, Wandinger U, Chaikovskaya L, Denisov S, Grudo J, Lopatin A, Karol Y, Lapyonok T, Amiridis V, Ansmann A, Apituley A, Allados-Arboledas L, Binietoglou I, Boselli A, D'Amico G, Freudenthaler V, Giles D, Granados-Muñoz MJ, Kokkalis P, Nicolae D, Oshchepkov S, Papayannis A, Rita PM, Pietruczuk A, Rocadenbosch F, Sicard M, Slutsker I, Talianu C, De Tomasi F, Tsekeri A, Wagner J & Wang X 2016. Lidar-Radiometer Inversion Code (LIRIC) for the retrieval of vertical aerosol properties from combined lidar/radiometer data: Development and distribution in EARLINET. *Atmos Measure. Tech.*, 9(3): 1181–1205. doi: 10.5194/amt-9-1181-2016.

Chen WN, Tsao CC & Nee JB 2004. Rayleigh lidar temperature measurements in the upper troposphere and lower stratosphere. *J. Atmos and Solar-Terrestrial Phy.*, 66(1): 39–49. doi: 10.1016/j.jastp.2003.09.014.

Collis RTH, Fernald FG & Ligda MGH 1964. Laser radar echoes from a stratified clear atmosphere. *Nature*, 203: 1274–1275.

Collis RTH & Russell PB 1976. Lidar measurement of particles and gases by elastic backscattering and differential absorption In: Laser Monitoring of the Atmosphere. Hinkley ED (ed.). *Topics in Applied Phy.*, vol 14. Springer, Berlin, Heidelberg, pp. 71-151.doi: 10.1007/3-540-07743-x_18.

Comerón A, Rocadenbosch F, López MA, Rodriguez A, Munoz C, García-Vizcaíno D & Sicard M 2004. Effects of noise on lidar data inversion with the backward algorithm.*Applied Opt.*, 43(12): 2572–2577. doi: 10.1364/AO.43.002572.

Comerón A, Muñoz-Porcar C, Rocadenbosch F, Rodríguez-Gómez A & Sicard M 2017. Current research in lidar technology used for the remote sensing of atmospheric aerosols. *Sensors*, 17:1-16. doi: 10.3390/s17061450.

Davis PA 1969. The analysis of lidar signatures of cirrus clouds. *Applied Opt.*, 8(10), 2099–2102. doi: 10.1364/ao.8.002099.

Dittrich PG, Bichra M, Pfützenreuter C, Rosenberger M & Notni G 2019. Measurement principle and arrangement for the determination of spectral channel-specific angle dependencies for multispectral resolving filter-on-chip CMOS cameras. *Joint TC1 - TC2 Inter. Symp. on Photonics and Edu. in Measue. Sci 2019 SPIE.,* 1–11. doi: 10.1117/12.2527871.

Dubovik O, Lapyonok T, Litvinov P, Herman M, Fuertes D, Ducos F, Torres B, Derimian Y, Huang X, Lopatin A, Chaikovsky A, Aspetsberger M & Federspiel C.2014. GRASP: A versatile algorithm for characterizing the atmosphere.*SPIE Newsroom*,: 2–5.

Fernald FG 1984. Analysis of atmospheric lidar observations : some comments. *Applied Opt.*, 23(5): 652-3.

Fernald FG, Herman BM & Reagan JA 1972. Determination of Aerosol Height Distributions by Lidar. *J. Applied Met.*, 11(3): 482–489. doi: 10.1175/1520-0450(1972)011<0482:doahdb>2.0.co;2.

Gimmestad GG 2008. Reexamination of depolarization in lidar measurements. *Applied Opt.*, 47(21): 3795–3802. doi: 10.1364/AO.47.003795.

Harms J 1979. Lidar return signals for coaxial and noncoaxial systems with central obstruction. *Applied Opt.*, 18(10): 1559-1565. doi: 10.1364/ao.18.001559.

Hey JV, Coupland J, Foo MH, Richards J & Sandford A 2011. Determination of overlap in lidar systems. *Applied Opt.*, 50(30): 5791–5797. doi: 10.1364/AO.50.005791.

Hitschfeld W & Bordan J 1954. Errors inherent in the radar measurement of rainfall at attenuating wavelengths. *J. Met.*, 11: 58–67.

Hoff RM, Guise-Bagle L, Staebler RM,Wiebe HA, Brook J, Georgi B & Dusterdiek, T1996. Lidar, nephelometer, and in situ aerosol experiments in southern Ontario.*J.l of Geophy. Research*, 101: 199-209.

IPCC 2001. Climate Change 2001: The Scientific Basis. Cambridge University Press: Cambridge, UK. doi: 10.1016/S1058-2746(02)86826-4.

Kaufman YJ, Koren I, Remer LA, Tanré D, Ginoux P & Fan S 2005. Dust transport and deposition observed from the Terra-Moderate Resolution Imaging Spectroradiometer (MODIS) spacecraft over the Atlantic Ocean. *J. Geophy Research D: Atmos.*, 110(10): 1–16. doi: 10.1029/2003JD004436.

Killinger DK & Menyuk N 1987. Laser remote sensing of the atmosphere. *Sci.*, 235(4784): 37–45. doi: 10.1126/science.235.4784.37.

Klett JD 1981. Stable analytical inversion solution for processing lidar returns. *Applied Opt.*, 20(2): 211-220. doi: 10.1364/ao.20.000211.

Klett JD 1985. Lidar inversion with variable backscatter/extinction ratios. *Applied Opt.*, 24(11): 1638-1643. doi: 10.1364/ao.24.001638.

Kong Z, Liu Z, Zhang L, Guan P, Li L & Mei L 2018. Atmospheric pollution monitoring in Urban area by employing a 450-nm lidar system. *Sensors (Switzerland)*, 18(6): 1880|1-12. doi: 10.3390/s18061880.

Kong Z, Ma T, Cheng Y, Zhang Z, Li Y, Liu K & Mei L 2020. Feasibility investigation of a monostatic imaging lidar with a parallel-placed image sensor for atmospheric remote sensing. *J. Quanti. Spect. and Rad. Transfer*, 254: 1072|1-12. doi: 10.1016/j.jqsrt.2020.107212.

Kovalev VA 2003. Stable near-end solution of the lidar equation for clear atmospheres. *Applied Opt.*, 42(3): 585-591. doi: 10.1364/ao.42.000585.

Kovalev VA & Eichinger WE 2005. Elastic Lidar. John Wiley & Sons, Inc., New Jersey USA. doi: 10.1002/0471643173.

Lihui L,Tianshu Z, Cheng L, Yunsheng D, Zhenyi C, Guangqiang F, Yang L & Wenqing L 2015. Atmospheric aerosols detection research with a dual field of view Lidar. *J. Spect.*, 1-6. doi: 10.1155/2015/459460.

Liu B *et al.* 2011. Development of a mobile Raman-Mie lidar system for all time water vapor and aerosol detection. *J. Quant. Spectro. and Radiative Transfer*, 112(2): 230–235. doi: 10.1016/j.jqsrt.2010.05.019.

Liu D, Yang Y, Cheng Z, Huang H, Zhang B, Ling T & Shen Y 2013. Retrieval and analysis of a polarized high-spectral-resolution lidar for profiling aerosol optical properties. *Opt. Exp.*, 21(11): 13084. doi: 10.1364/oe.21.013084.

Liu J, Chen W, Zhu X, Zhu X, Zhang X, Liu Y & Shi W 2016. Development of 1.5 μm all-fiber pulsed coherent Doppler wind lidar. *18th Coherent Laser Radar Conference and the Lidar Working Group on Space Based Winds, CLRC*, pp. 8–11.

Liu Z, Li L, Li H & Mei L 2019. Preliminary studies on atmospheric monitoring by employing a portable unmanned mie-scattering Scheimpflug lidar system. *Rem. Sensing*, 11(7): 837|1-17. doi: 10.3390/RS11070837.

Lolli S, Sauvage L, Loaec S & Lardier M 2011. EZ Lidar™: A new compact autonomous eye-safe scanning aerosol Lidar for extinction measurements and PBL height detection. Validation of the performances against other instruments and intercomparison campaigns. *Optica Pura y Aplicada*, 44(1): 33–41.

Lopatin A, Dubovik O, Chaikovsky A, Goloub P, Lapyonok T, Tanré D & Litvinov P 2013. Enhancement of aerosol characterization using synergy of lidar and sun-

FUW Trends in Science & Technology Journal, www.ftstjournal.com
e-ISSN: 24085162; p-ISSN: 20485170; December, 2021: Vol. 6 No. 3 pp. 713 – 721

719

photometer coincident observations: The GARRLiC algorithm. *Atmos. Meas. Tech.*, 6(8): 2065–2088. doi: 10.5194/amt-6-2065-2013.

Madonna F, Amato F, Hey JV & Pappalardo G 2015. Ceilometer aerosol profiling versus Raman lidar in the frame of the INTERACT campaign of ACTRIS. *Atmos Meas. Tech.*, 8(5): 2207–2223. doi: 10.5194/amt-8-2207-2015.

Marchant CC, Wilkerson TD, Bingham GE, Zavyalov VV, Andersen JM, Wright CB, Cornelsen SS, Martin RS, Silva PJ & Hatfield JL 2009. Aglite lidar: a portable elastic lidar system for investigating aerosol and wind motions at or around agricultural production facilities. *J. Applied Rem. Sensing*, 3(1): 1-20. doi: 10.1117/1.3097928.

Mattis I, Ansmann A, Müller D, Wandinger U & Althausen D 2004. Multilayer aerosol observations with dual-wavelength Raman lidar in the framework of EARLINET. *J. of Geophys.Research D: Atmos.*, 109(13): 1–15. doi: 10.1029/2004JD004600.

Mei L, Guan P, Yang Y & Kong Z 2017. Atmospheric extinction coefficient retrieval and validation for the single-band Mie-scattering Scheimpflug lidar technique. *Opt. Exp.*, 25(16): A628-A638. doi: 10.1364/oe.25.00a628.

Mei L, Zhang L, Kong Z & Li H 2018. Noise modeling, evaluation and reduction for the atmospheric lidar technique employing an image sensor. *Opt Comm.*, 426: 463–470. doi: 10.1016/j.optcom.2018.05.072.

Mei L, Ma T, Kong Z, Gong Z & Li H 2019. Comparison studies of the Scheimpflug lidar technique and the pulsed lidar technique for atmospheric aerosol sensing. *Applied Opt.,* 58(32): 8981-8992. doi: 10.1364/ao.58.008981.

Mei L, Li L, Liu Z, Fei R, Lu Q, Chen K & Gong ZF 2019. Detection of the planetary boundary layer height by employing the Scheimpflug lidar technique and the covariance wavelet transform method. *Applied Opt.*, 58(29): 8013-8020. doi: 10.1364/ao.58.008013.

Mei L & Brydegaard M 2015a. Atmospheric aerosol monitoring by an elastic Scheimpflug lidar system. *Opt. Exp.*, 23(24): A1613-A1628. doi: 10.1364/oe.23.0a1613.

Mei L & Brydegaard M 2015b. Continuous-wave differential absorption lidar. *Laser and Photonics Rev*, 9(6): 629–636. doi: 10.1002/lpor.201400419.

Mei L & Brydegaard M 2016. Development of a scheimpflug lidar system for atmospheric aerosol monitoring. *EPJ Web Conf.*, 119: 4–7. doi: 10.1051/epjconf/201611927005.

Mei L & Guan P 2017. Development of an atmospheric polarization Scheimpflug lidar system based on a time-division multiplexing scheme. *Opt. Letters*, 42(18): 3562-3265. doi: 10.1364/ol.42.003562.

Mei L, Kong Z & Guan P 2018. Implementation of a violet Scheimpflug lidar system for atmospheric aerosol studies. *Opt. Exp.*, 26(6): A260-A274. doi: 10.1364/oe.26.00a260.

Mei L, Kong Z & Ma T 2018. Dual-wavelength Mie-scattering Scheimpflug lidar system developed for the studies of the aerosol extinction coefficient and the Ångström exponent. *Opt. Exp.*, 26(24): 31942-31956. doi: 10.1364/oe.26.031942.

Meki K 1996. Range-resolved bistatic imaging lidar for the measurement of the lower atmosphere. *Opt. Letters*, 21(17): 1318-1320. doi: 10.1364/ol.21.001318.

Moorgawa A, Bencherif H, Michaelis MM, Porteneuve J & Malinga S 2007. The Durban atmospheric LIDAR. *Opt. and Laser Tech.*, 39(2): 306–312. doi: 10.1016/j.optlastec.2005.07.014.

Pal S, Behrendt A, Radlach M, Schaberl T & Wulfmeyer V 2006. Eye-safe scanning aerosol lidar at 355 nm. *Proc. of the 23rd Inter. Laser Radar Conf.*, 797–800. Nara, Japan.

Pal SR, Steinbrecht W & Carswell AI 1992. Automated method for lidar determination of cloud-base height and vertical extent. *Applied Opt.*, 31(10): 1488-1494. doi: 10.1364/ao.31.001488.

Pedrós R, Estellés V, Sicard M, Gómez-Amo JL, Utrillas MP, Martínez-Lozano JA, Rocadenbosch F, Pérez C&Recio BJM 2010. Climatology of the aerosol extinction-to-backscatter ratio from sun-photometric measurements. *IEEE Trans on Geosci. and Rem. Sensing*, 48(1): 237–249. doi: 10.1109/TGRS.2009.2027699.

Potter JF 1987. Two-frequency lidar inversion technique. *Applied Opt.*, 26(7): 1250-1256. doi: 10.1364/ao.26.001250.

Rocadenbosch F, Frasier S, Kumar D, Lange VD, Gregorio E & Sicard M 2012. Backscatter error bounds for the elastic lidar two-component inversion algorithm. *IEEE Trans. on Geosci. and Rem. Sensing*, 50(11): 4791–4803. doi: 10.1109/TGRS.2012.2194501.

Sharma NCP, Barnes JE, Kaplan TB & Clarke AD 2011. Coastal aerosol profiling with a camera lidar and nephelometer. *J. Atmos. and Oceanic Tech.*, 28(3): 418–425. doi: 10.1175/2010JTECHA1482.1.

Shimizu A, Sugimoto N, Matsui I, Arao K, Uno I, Murayama T, Kagawa N, Aoki K, Uchiyama A & Yamazaki AA 2004. Continuous observations of Asian dust and other aerosols by polarization lidars in China and Japan during ACE-Asia.*J. of Geophy. Research D: Atmos.*, 109(19): D19S17|1-14. doi: 10.1029/2002JD003253.

Sicard M, Chazette P, Pelon J, Won JG & Yoon SC 2002. Variational method for the retrieval of the optical thickness and the backscatter coefficient from multiangle lidar profiles. *Applied Opt.*, 41(3): 493-502. doi: 10.1364/ao.41.000493.

Soriano C, Buttler WT & Baldasano JM 1995. Comparison of temperature and humidity profiles with elastic-backscatter lidar data. *Proc. Intern. Conf. on Air Pol.*, 275–282.

Sroga JT, Eloranta EW & Barber T 1980. Lidar measuremnt of wind velocity profiles in the boundary layer. *J. Applied Meteo*, 19: 598–605. doi: 10.1088/1751-8113/44/8/085201.

Stelmaszczyk K, Aglio MD & Chudzyn S 2005. compression form-factor calculations .*Applied Opt.*, 44(7): 1323–1331.

Strawbridge KB 2013. Developing a portable, autonomous aerosol backscatter lidar for network or remote operations. *Atmos. Measure. Tech.*, 6(3): 801–816. doi: 10.5194/amt-6-801-2013.

Stull RB 1988. An introduction to boundary layer meteorology. Kluwer Academic Publishers, London UK.doi:10.1007/978-94-009-3027-8.

Sun G, Qin L, Hou Z, Jing X, He F, Tan F & Zhang S 2018. Small-scale Scheimpflug lidar for aerosol extinction coefficient and vertical atmospheric transmittance detection. *Opt. Exp.*, 26(6): 74237436. doi: 10.1364/oe.26.007423.

Takeuchi N 2005. Elastic Lidar Measurement of the Troposphere In: Laser Remote Sensing. Fujii T & Fukuchi T (ed.). CRC Press, Taylor & Francis Group, New York, p. 63–122. doi: 10.1111/j.1477-9730.2006.00406_2.x.

Tao Z, Liu D, Wang Z, Ma X, Zhang Q, Xie C, Bo G, Hu S & Wang Y 2014. Measurements of aerosol phase function and vertical backscattering coefficient using a charge-coupled device side-scatter lidar. *Opt. Exp.*, 22(1): 1127-1134. doi: 10.1364/oe.22.001127.

FUW Trends in Science & Technology Journal, www.ftstjournal.com
e-ISSN: 24085162; p-ISSN: 20485170; December, 2021: Vol. 6 No. 3 pp. 713 – 721

720

Tesche M, Ansmann A, Müller D, Althausen D, Engelmann R, Freudenthaler V & Groß S 2009. Vertically resolved separation of dust and smoke over Cape Verde using multiwavelength Raman and polarization lidars during Saharan mineral dust experiment 2008. *J. Geophy. Res. Atmos.*, 114(13): 1–14. doi: 10.1029/2009JD011862.

Vaughan G, Wareing DP, Thomas L & Mitev V 1988. Humidity measurements in the free troposphere using Raman backscatter. *Quarterly J. Royal Met. Soc.*, 114(484): 1471–1484. doi: 10.1002/qj.49711448406.

Wandinger U, Müller D, Böckmann C, Althausen D, Matthias V, Bösenberg J, Weiß V, Fiebig M, Wendisch M, Stohl A & Ansmann A 2002. Optical and microphysical characterization of biomass-burning and industrial-pollution aerosols from multiwavelength lidar and aircraft measurements. *J Geophy. Res. Atmos.*, 107(21): 1-20 doi: 10.1029/2000JD000202.

Wandinger U 2005. Introduction to Lidar In:Lidar Range-Resolved Optical Remote Sensing of the Atmosphere. Weitkamp C (ed.). Springer: New York, NY, USA, p. 1–18.

Wandinger U, Hiebsch A, Mattis I, Pappalardo G, Mona L & Madonna F 2011. Aerosols and Clouds, Long-term Database from Spaceborne Lidar Measurements.*Final report, ESTEC Contract 21487/08/NL/HE*, (June).

Wiegner M, Madonna F, Binietoglou I, Forkel R, Gasteiger J, Geiß A, Pappalardo G, Schäfer K & Thomas W 2014. What is the benefit of ceilometers for aerosol remote sensing? An answer from EARLINET. *Atmos Measure. Tech.*, 7(7): 1979–1997. doi: 10.5194/amt-7-1979-2014.

Xie C, Zhao M, Wang B, Zhong Z, Wang L, Liu D & Wang Y 2015. Study of the scanning lidar on the atmospheric detection. *J. Quant. Spect. and Radiative Trans.*, 150: 114–120. doi: 10.1016/j.jqsrt.2014.08.023.

Xu J, Liu D, Wang Z, Wu D, Yu S & Wang Y 2019. A study of the characteristics of vertical cloud base height distribution over Eastern China. *Atmos.*, 10(6): 1-11 doi: 10.3390/atmos10060307.

Zhao G, Malmqvist E, Török S, Bengtsson PE, Svanberg S, Bood J & Brydegaard M 2018. Particle profiling and classification by a dual-band continuous-wave lidar system. *Applied Opt.*, 57(35): 10164-10171. doi: 10.1364/ao.57.010164.

FUW Trends in Science & Technology Journal, www.ftstjournal.com
e-ISSN: 24085162; p-ISSN: 20485170; December, 2021: Vol. 6 No. 3 pp. 713 – 721

721